Novel Structure Evolution of Lanthanide–SIP Coordination Polymers (NaH_2SIP = 5-Sulfoisophthalic Acid Monosodium Salt) from a 1D Chain to a 3D Network as a Consequence of the Lanthanide Contraction Effect

Qing-Yan Liu[a,b] and Li Xu*[a]

Keywords: Crystal structures / Hydrothermal synthesis / Lanthanides / Lanthanide contraction

The new series of lanthanide–SIP coordination polymers $[\{Ln(SIP)(H_2O)_5\}(H_2O)_3]_n$ (Ln = Lu (**1**), Yb (**2**), Tm (**3**), and Er (**4**)], $[\{Ln(SIP)(H_2O)_4\}]_n$ (Ln = Ho (**5**), Dy (**6**), Tb (**7**), Sm (**8**), Pr (**9**), and Nd (**10**)], and $[\{La(SIP)(H_2O)_3\}(H_2O)]_n$ (**11**), have been synthesized by hydrothermal reactions of Ln_2O_3 and 5-sulfoisophthalic acid monosodium salt (NaH_2SIP) at 160 °C and characterized by single-crystal X-ray diffraction. The unprecedented three structure types ongoing from Lu^{III} to La^{III} have been established: type I for the small ions, Lu, Yb, Tm, and Er; type II for the medium ions including Ho, Dy, Tb, Sm, Pr, and Nd; and type III for the largest La ion. Type I adopts a one-dimensional zigzag chain-like structure, type II exhibits a two-dimensional undulate layer structure, and type III features a two-dimensional double-layer pillared by sulfonate groups to form a three-dimensional open framework. The progressive structural changes from type I to type II and to type III with increasing atomic number were rationalized by the effect of the lanthanide contraction. Their spectroscopic properties and thermal stability were also investigated.

Introduction

The design and construction of coordination polymers is one of the most active areas of materials research. The intense interest in these materials is driven by both their interesting network topologies and their potential applications in catalysis, molecular magnets, sensors, ion exchange, adsorption, and phase separation.[1–6] Numerous coordination polymers with varied dimensions and topologies have been obtained through a judicious choice of organic linkers and metal ions.[7–14] Many of the efforts have so far been devoted to the study of transition-metal-based coordination polymers.[15–19] The chemistry of lanthanide coordination polymers has been less-well investigated despite their useful luminescent, catalytic, and magnetic properties.[20–25] For example, our knowledge about how the lanthanide contraction works in crystal-structure formation is limited because of few systematic investigations across the lanthanide series with a single ligand.[26–28] This contribution deals with the self-assembly of the lanthanide series with the single SIP ligand. SIP was selected for several reasons: (1) it contains a soft sulfonate group that may serve as a more sensitive probe in the exploration of the effect of the lanthanide contraction; (2) it has three functional groups that allow the formation of structures of higher dimensions; (3) π–π stacking interactions between the aromatic rings may facilitate ordered, noninterpenetrated open frameworks; (4) it has an asymmetric geometry that may lead to acentric crystal structures that are needed for the development of non-linear optical materials. This new series of lanthanide–SIP coordination polymers prepared by hydrothermal reactions displays three types of polymeric structures, ranging from one-dimensional chains to a three-dimensional framework on going from Lu to La.

[a] State Key Laboratory of Structural Chemistry, Fujian Institute of Research on the Structure of Matter, Chinese Academy of Sciences,
Fuzhou, Fujian, 350002, P. R. China
Fax: +86-591-8370-5045
E-mail: xli@fjirsm.ac.cn
[b] Graduate School of the Chinese Academy of Sciences,
Beijing 100039, P. R. China
Fax: +86-591-8370-5045
E-mail: qyliu@fjirsm.ac.cn
Supporting information for this article is available on the WWW under http://www.eurjic.org or from the author.

Results and Discussion

Preparation of the Complexes

We prepared the series of Ln^{III}–SIP compounds **1**–**11** with the structures $[\{Ln(SIP)(H_2O)_5\}(H_2O)_3]_n$ [Ln = Lu (**1**), Yb (**2**), Tm (**3**), and Er (**4**)], $[\{Ln(SIP)(H_2O)_4\}]_n$ [Ln = Ho (**5**), Dy (**6**), Tb (**7**), Sm (**8**), Pr (**9**), and Nd (**10**)], and $[\{La(SIP)(H_2O)_3\}(H_2O)]_n$ (**11**) (excluding the rare and radioactive Pm as well as Eu^{III} and Gd^{III} reported previously[29]) by a hydrothermal reaction of Ln_2O_3 and NaH_2-SIP in aqueous solution. The preparative reactions were carried out at different temperatures (140 °C, 160 °C, and 180 °C) to investigate the temperature dependence of their solid structures. X-ray diffraction analyses of the products

  DOI: 10.1002/ejic.200500271

indicated that the same results were obtained at these reaction temperatures although the purity and yields were slightly different, indicative of the thermodynamic nature of the hydrothermal reactions. Attempts to get single crystals of the Ce–SIP compound by reacting CeO_2 with NaH_2SIP were unsuccessful. This compound has been reported previously but the crystal structure was not determined. The crystalline compounds **1**–**11** could not be isolated from the conventional reaction of Ln_2O_3 with NaH_2SIP in aqueous solution at room temperature, indicating the kinetic nature of the reactions. The different results between the conventional solutions and hydrothermal reactions may be caused by a different reaction mechanism: the hydrothermal reaction mechanism is shifted from the kinetic to the thermodynamic domain when compared to a conventional solution reaction.[30–32]

Table 1. Selected bond lengths [Å] for compounds **1**–**4**.[a]

	Lu (**1**)	Yb (**2**)	Tm (**3**)	Er (**4**)
Ln–O1	2.392(11)	2.401(15)	2.415(5)	2.415(3)
Ln–O2	2.443(11)	2.438(16)	2.463(6)	2.447(3)
Ln–O3A	2.392(12)	2.406(16)	2.410(5)	2.463(3)
Ln–O4A	2.443(13)	2.456(16)	2.437(5)	2.423(3)
Ln–O8	2.285(13)	2.291(17)	2.306(6)	2.310(3)
Ln–O9	2.297(12)	2.306(16)	2.315(6)	2.326(3)
Ln–O10	2.300(13)	2.314(16)	2.321(6)	2.333(3)
Ln–O11	2.360(13)	2.370(19)	2.385(7)	2.393(3)
Ln–O12	2.455(13)	2.468(16)	2.471(6)	2.460(3)
Ln–O (av.)	2.374	2.383	2.391	2.397
O···O (av.)	2.857	2.864	2.856	2.686
π–π interacting distances (face-to-face)	3.715	3.705	3.715	3.687
Dihedral angle of benzene rings in the chain [°]	51.0	51.4	51.7	48.4

[a] Symmetry transformation for equivalent atoms: A: $x - 1/2, -y + 1/2, z - 1/2$.

Crystal Structures

The X-ray diffraction analyses of compounds **1**–**11** revealed three types of solid structures on going from Lu to La: a 1D chain (**1**–**4**, Lu–Er), a 2D sheet (**5**–**10**, Ho–Pr), and a 3D network (**11**, La). These structure types result from the different coordination modes of SIP, as illustrated in Scheme 1, presumably as a consequence of the lanthanide contraction, as will be detailed below.

Type I: Structure of $[\{Ln(SIP)(H_2O)_5\}(H_2O)_3]_n$ [Ln = Lu (1), Yb (2), Tm (3), and Er (4)]

The type I structure features a one-dimensional ribbon, as exemplified in Figure 1 for **4** (Ln = Er). Each Er^{III} ion is coordinated to nine oxygen atoms, four from the carboxylate groups and five from water molecules (Figure 1a). SIP uses the two carboxylate arms to chelate to the Er^{III} ions, as illustrated in Scheme 1(a), to form an infinite zigzag chain (Figure 1b). The Er–O distances given in Table 1 range from 2.310(3) to 2.463(3) Å (average value 2.397 Å). The phenyl rings in the chain are not parallel but are twisted relative to each other with a dihedral angle of around 48.4°. The uncoordinated sulfonate group forms hydrogen bonds with coordinated and lattice water molecules.

The extensive interchain hydrogen bonds link the zigzag chains into a three-dimensional supramolecular layer structure, as illustrated in Figure 2. Two types of hydrogen bonds are observed between the chains: hydrogen bonds between the coordinated water molecules and carboxylate oxygen atoms (O···O = 2.723–2.900 Å), and hydrogen bonds between the coordinated water molecules and sulfonate oxygen atoms (O···O = 2.675, 2.814, and 2.929 Å). The supramolecular layer structures are further stabilized by π–π interactions between the parallel aromatic rings in an off-set fashion, with a face-to-face distance of about 3.687 Å. Similar hydrogen bonds and π–π interactions between aromatic rings have also been reported in the cadmium complexes recently reported.[33,34] The lattice water molecules located in the cavities of the supramolecular open framework are hydrogen bonded to each other and the chain, with O···O distances ranging from 2.703 to 3.081 Å.

The Lu (**1**), Yb (**2**), and Tm (**3**) complexes possess a similar structure. Selected bond lengths, hydrogen bonds, and π–π stacking distances between aromatic rings are listed in Table 1. The results indicate that the Ln–O bond lengths increase from Lu (**1**) to Er (**4**), as expected for the lanthanide contraction.

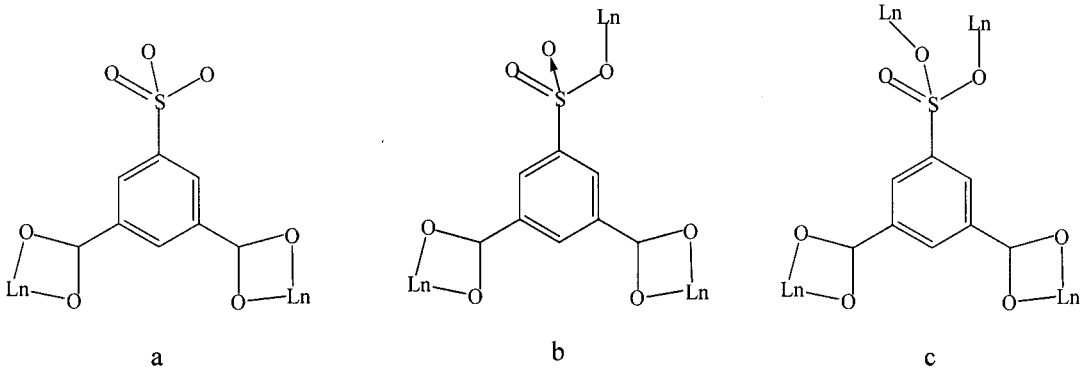

Scheme 1. The three different coordination modes of the SIP ligand observed in complexes **1**–**11**.

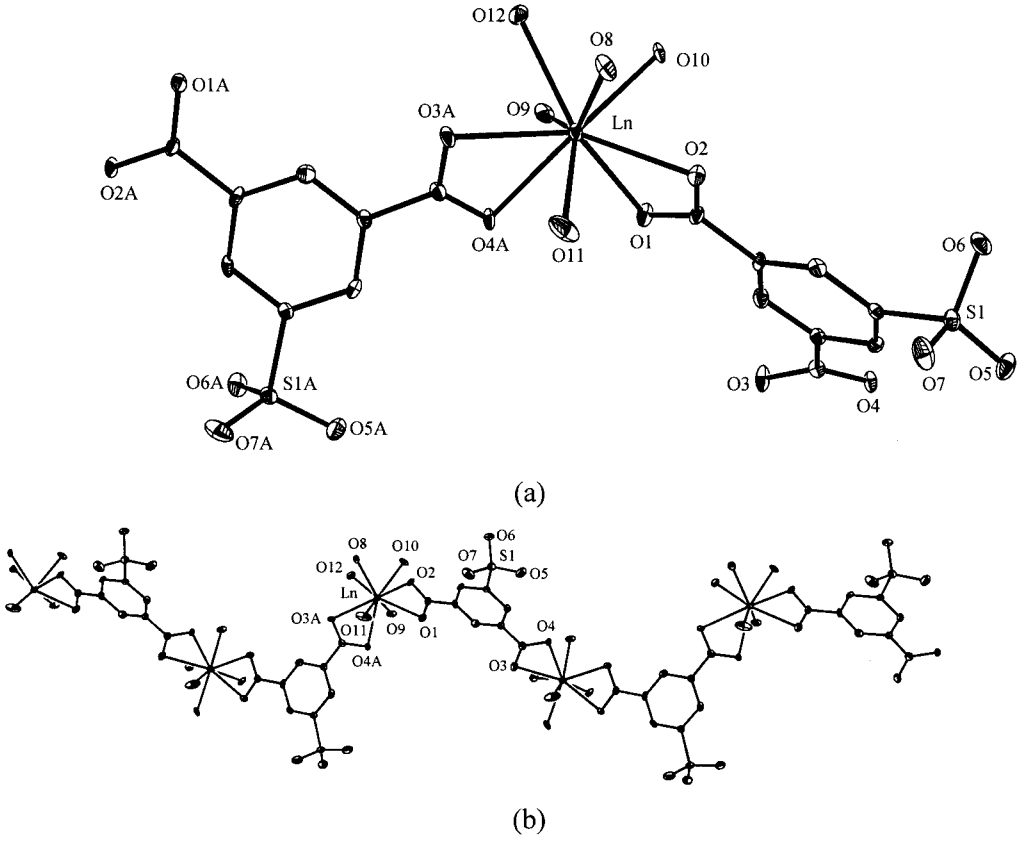

Figure 1. a) Local coordination environment of the lanthanide ions [Ln = Lu (**1**), Yb (**2**), Tm (**3**), and Er (**4**)]. b) Infinite zigzag chain of complexes **1**–**4**.

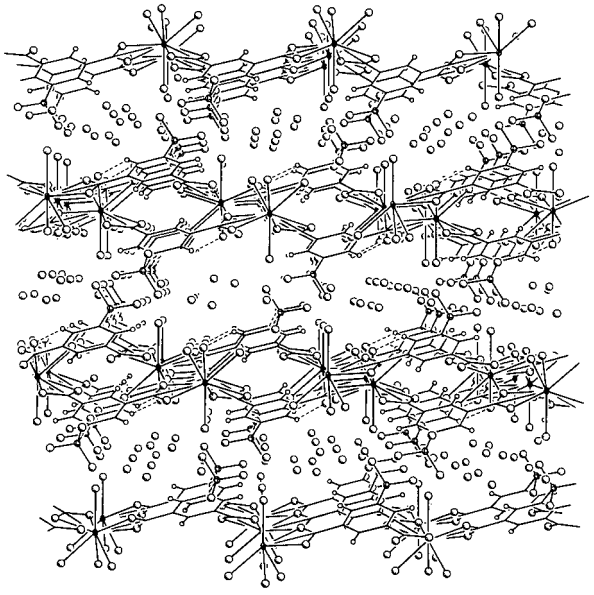

Figure 2. Three-dimensional supramolecular framework of **1**–**4**. The lattice water molecules occupy the interlayer space. The interlamellar interactions between the neighboring layers are hydrogen bonds (not shown).

Type II: Structure of [{Ln(SIP)(H$_2$O)$_4$}]$_n$ [Ln = Ho (5), Dy (6), Tb (7), Sm (8), Pr (9), and Nd (10)]

The lanthanide ions Ho (**5**), Dy (**6**), Tb (**7**), Sm (**8**), Pr (**9**), and Nd (**10**) form type II structures with the acentric crystal system, space group $Pna2_1$. They have similar crystal structures, as displayed in Figure 3a for Ln = Pr. Their selected bond lengths, hydrogen bonds, and π–π stacking distances are listed in Table 2. The type II structure can be described as an undulating, two-dimensional, sheet-like structure constructed from fused $[Pr(SIP)_3(H_2O)_4]$ pseudo-hexagonal grids (Figure 3b). The tridentate SIP ligand links the three surrounding Pr^{III} atoms through two chelating carboxylate groups and one sulfonate oxygen atom, as illustrated in Scheme 1(b). The presence of intermolecular hydrogen bonds and π–π interactions finally results in a three-dimensional supramolecular structure, as depicted in Figure 4. Compounds **5**–**10** are isomorphous with the previously reported Eu^{III} and Gd^{III} complexes.[29] A structural comparison with type I compounds may give an insight into the formation of type II species. Both types of compounds have nine-coordinate lanthanide ions in a similar coordination geometry. The type II structure may best be understood as resulting from interchain replacement of one of the coordinated waters by one sulfonate oxygen atom in a type I structure. The resultant Ln–O_3S bonding links the

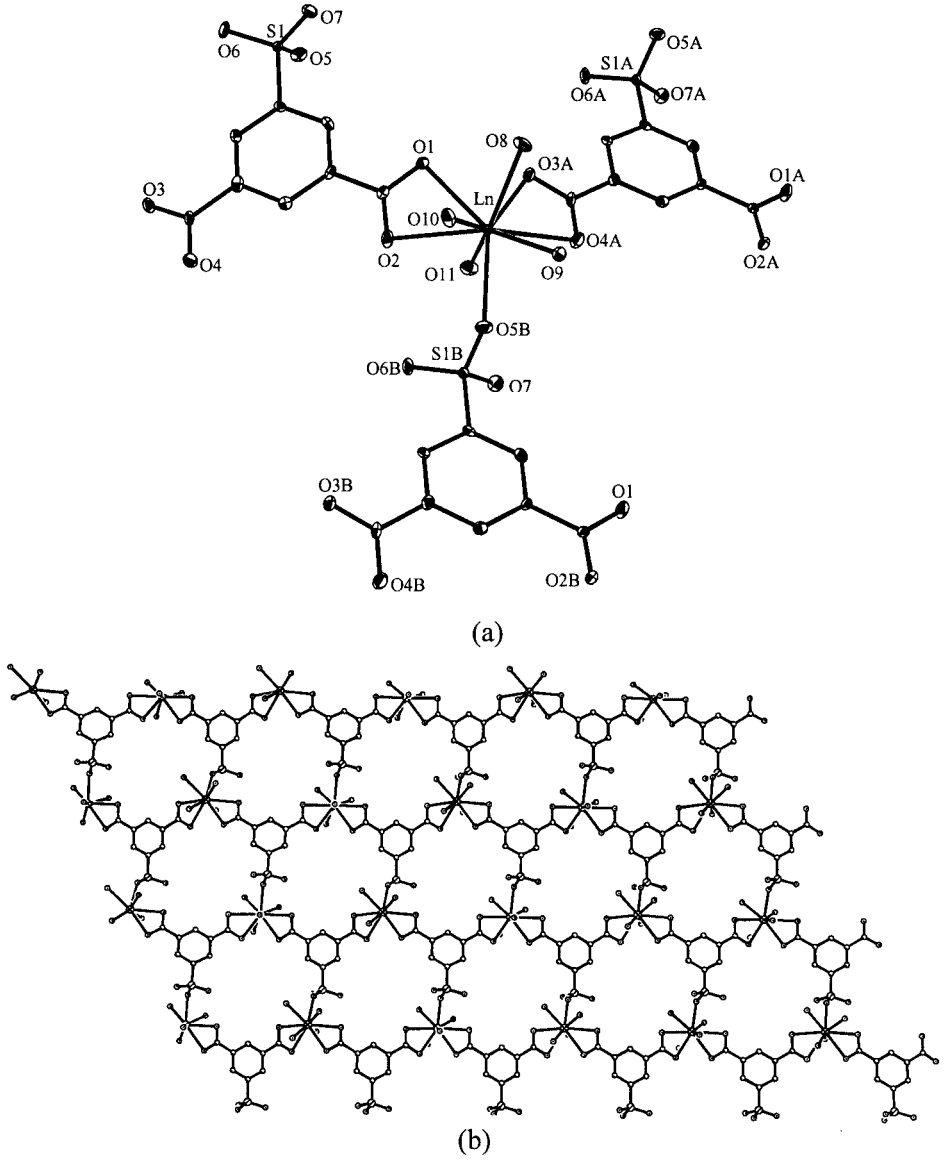

Figure 3. a) Local coordination environment of the lanthanide ions [Ln = Ho (**5**), Dy (**6**), Tb (**7**), Sm (**8**), Pr (**9**), and Nd (**10**)]. b) Two-dimensional network structure of complexes **5–10**.

Table 2. Selected bond lengths [Å] for compounds **5–9**.[a]

	Ho (**5**)	Dy (**6**)	Tb (**7**)	Sm (**8**)	Pr (**9**)
Ln–O1	2.415(8)	2.466(12)	2.442(5)	2.502(18)	2.519(4)
Ln–O2	2.494(7)	2.539(14)	2.504(5)	2.540(16)	2.560(3)
Ln–O3A	2.436(7)	2.472(10)	2.462(4)	2.476(16)	2.536(3)
Ln–O4A	2.491(6)	2.550(11)	2.520(4)	2.541(15)	2.579(3)
Ln–O5B	2.384(7)	2.447(12)	2.409(5)	2.460(18)	2.476(4)
Ln–O8	2.363(9)	2.434(15)	2.392(7)	2.409(19)	2.472(4)
Ln–O9	2.375(8)	2.451(11)	2.400(4)	2.439(15)	2.482(3)
Ln–O10	2.376(6)	2.469(14)	2.403(6)	2.469(18)	2.517(3)
Ln–O11	2.420(5)	2.496(10)	2.434(4)	2.491(14)	2.541(3)
Ln–O (av.)	2.417	2.480	2.441	2.481	2.520
O···O (av.)	2.863	2.866	2.845	2.884	2.847
π–π distance	3.652	3.686	3.588	3.681	3.636
Dihedral angle [°]	8.0	6.9	8.1	8.6	7.2

[a] Symmetry transformation for equivalent atoms: A: $-x + 1/2$, $y + 1/2$, $z - 1/2$; B: $-x + 1/2$, $y + 1/2$, $z + 1/2$.

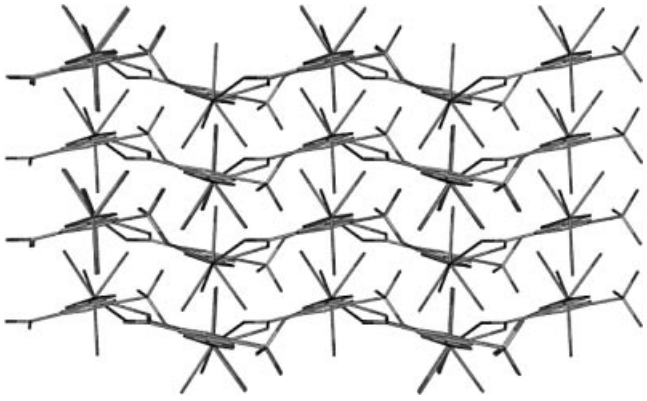

Figure 4. View of complexes **5–10** along the *b* axis. The interlayer interactions between the neighboring layers are hydrogen bonds (not shown).

zigzag chains into a 2D sheet. Such structure evolution suggests a stronger trend for the type II lanthanide ions to bind to anionic sulfonate groups, as will be detailed later.

Type III: 3D Open Framework Structure of [{La(SIP)-$(H_2O)_3$}(H_2O)]$_n$ (11)

Only lanthanum, which has the largest ionic radius in the lanthanide series, was found to form a 3D coordination polymer, namely [{La(SIP)$(H_2O)_3$}(H_2O)]$_n$ (**11**). As shown in Figure 5a, each La^{III} ion is coordinated by nine oxygen atoms, six from five SIP ligands and three from water molecules. The five SIP ligands are coordinated to the La^{III} center in three distinct modes, two by one carboxylate oxygen, two through one sulfonate oxygen, and one by a chelating carboxylate group. The La–O distances (Table 3) range from 2.451(5) to 2.596(5) Å (av. 2.544 Å), with the longest La–O distance associated with the sulfonate oxygen atoms. The S–O bond lengths are normal[35] [1.439(5), 1.443(5) and 1.446(5) Å] and similar to each other, as expected for the strong conjugation of sulfonate. As shown in Scheme 1 (c), SIP functions as an unprecedented hexadentate ligand with only one sulfonate oxygen atom uncoordinated. Of the three functional groups of SIP, one chelating carboxylate group and one unidentate oxygen atom of sulfonate group, together with the similar ones from a neighboring SIP, connect the two neighboring La^{III} ions to form the sixteen-

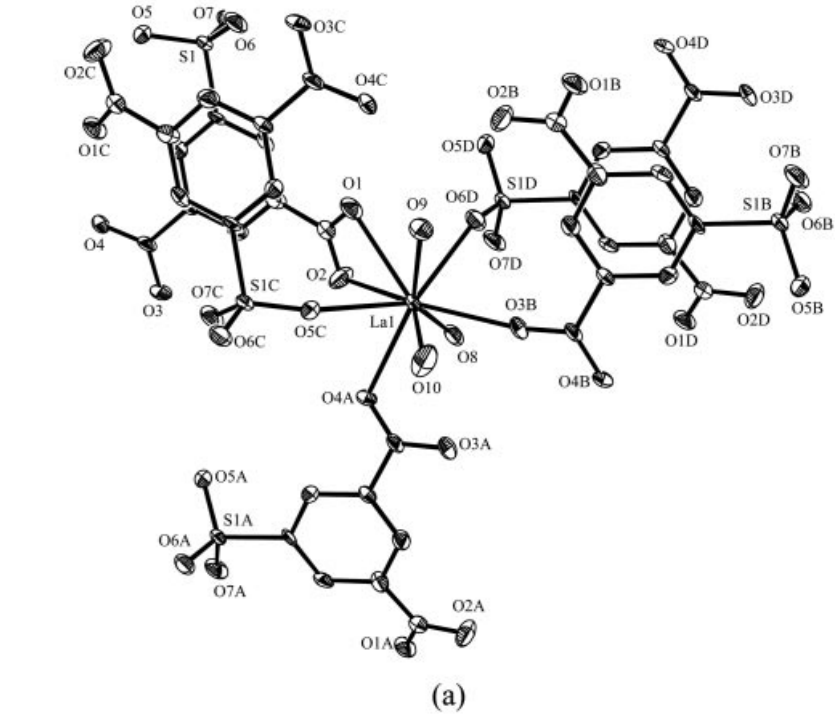

(a)

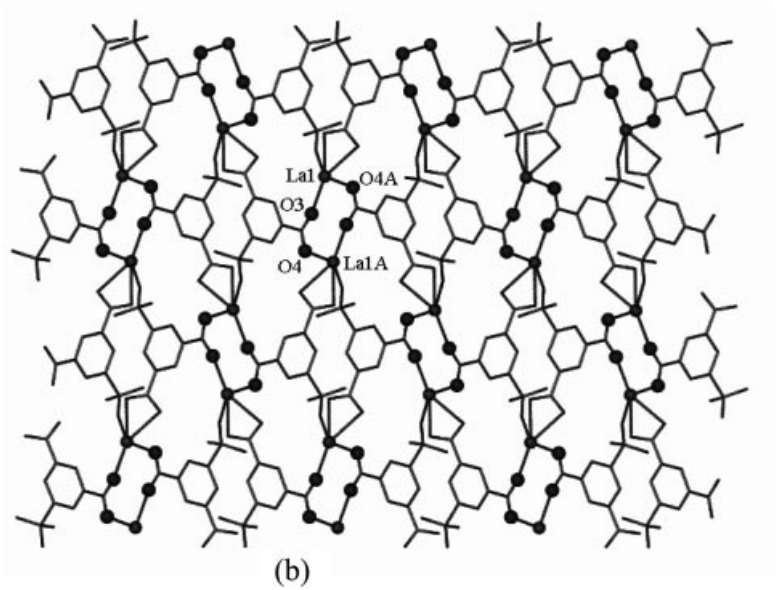

(b)

Figure 5. a) Local coordination environment of compound **11**. b) Two-dimensional sheet-like structure viewed along the *a* axis.

membered ring depicted in Figure 5b. Of interest is the other carboxylate group, which, together with the similar one from neighboring SIP, bridges a pair of La^{III} ions to form an $[La_2O_4C_2]$ eight-membered ring with an La···La separation of 4.982 Å, as shown in Figure 5a. Two types of rings connected by SIP propagate along the crystallographic *bc* plane to yield a two-dimensional sheet-like structure (Figure 5a). As described above, SIP uses five of its six donor atoms to form a 2D sheet. The sixth donor atom from the sulfonate group functions as a linker between the layers to form a 3D open framework, as depicted in Figure 6, with an approximate interlamellar separation of 3.884 Å. The free oxygen atom of the sulfonate group is involved in hydrogen bonding with the coordinated water molecules at a distance of 2.687–2.968 Å. The lattice water molecules are located in the cavities of the structure, forming a number of hydrogen bonds with carboxylate oxygen atoms, sulfonate oxygen atoms, and coordinated water molecules (O···O = 2.596–2.991 Å). The coordination polymer is further stabilized by π–π stacking interactions between the parallel aromatic rings in an off-set fashion, with a face-to-face distance of about 3.517 and 3.642 Å.

Table 3. Selected bond lengths [Å] for compound **11**.[a]

Bond	Distance [Å]	Bond	Distance [Å]
Ln–O1	2.583(5)	Ln–O2	2.586(5)
Ln–O3A	2.468(5)	Ln–O4B	2.507(4)
Ln–O5C	2.565(5)	Ln–O6D	2.596(5)
Ln–O8	2.451(5)	Ln–O9	2.565(5)
Ln–O10	2.574(5)	Ln–O (av.)	2.544

[a] Symmetry transformation for equivalent atoms: A: $x - 1/2, -y + 1/2, z - 1/2$; B: $-x + 1/2, y + 1/2, -z + 5/2$; C: $-x, -y, -z + 2$; D: $-x + 1/2, y + 1/2, -z + 3/2$.

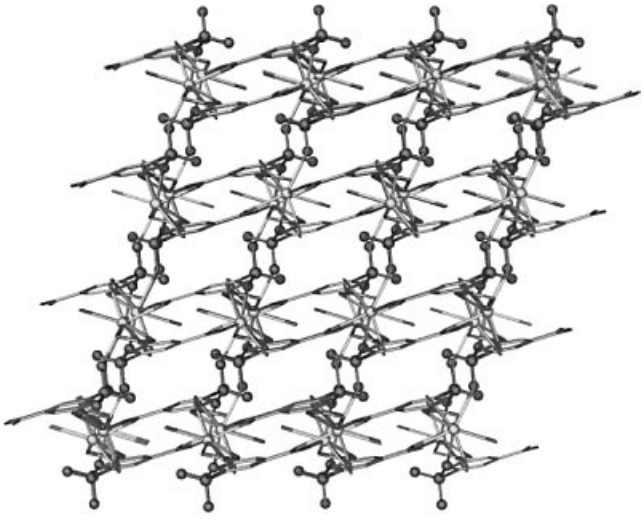

Figure 6. Three-dimensional pillared structure of complex **11** viewed along the *b* axis (the sulfonate groups and lanthanum atoms are represented as spheres).

Discussion of Structure Evolution

The self-assembly of the lanthanide series with a single ligand was found to form three unprecedented types of structures, ranging from a 1D chain to a 2D sheet and a 3D framework, wherein all lanthanide ions are nine-coordinate and trivalent. This intriguing structure evolution across the lanthanide series may be attributable to the effect of the lanthanide contraction. The structure evolution (from Lu to La) results from the extent to which the coordinated water molecules are replaced by the sulfonate oxygen atoms of the SIP ligand. Thus, the effect of the lanthanide contraction should be responsible for the water substitution with the sulfonate anions during the structure evolution. The preference to bond to anionic ligands can be measured as follows:

$$\Phi = Z/r$$

where Φ is the basicity, Z is the oxidation state, and r is the ionic radius.[36]

La^{III} has the largest ionic radius and thus the smallest basicity in the lanthanide(III) series. In other words, La^{III} has the greatest tendency to form La^{III}–O_3S bonds, thus accounting for the replacement of water by one sulfonate oxygen during the 2D → 3D structure evolution. Moreover, the large ionic radius allows the presence of five surrounding SIP ligands. The lighter lanthanide ions from Ho^{III} to Pr^{III} adopt a 2D sheet-like structure as a consequence of both their slightly higher basicity and smaller ionic radii. The lightest four lanthanide ions (Lu^{III}–Er^{III}) show no substantial interactions with the sulfonate oxygen donor atoms in their chain-like structures, consistent with their larger basicity and smallest radii. In summary, the sulfonate group of SIP is a comparatively soft oxygen donor ligand and is thus able to serve as a more sensitive probe for investigating the effect of the lanthanide contraction in crystal-structure formation of the lanthanide series, thereby accounting for the unprecedented three structure types observed in this lanthanide–SIP system.

FT-IR Spectra and Thermogravimetric Analyses

The FT-IR spectra of these complexes exhibit broad absorption bands in the range 3500–3200 cm^{-1} due to the presence of water molecules in the structures. The strong bands at 1360–1670 cm^{-1} for all complexes are characteristic of the carboxylate group. The absorptions in the region 1000–1230 cm^{-1} for all complexes are typical of the sulfonate group.[37] Interestingly, the characteristic bands of the carboxylate group show some changes from type I to type II, even though the coordination mode of the carboxylate groups in the two structure types is identical. In the type I structure these peaks are observed in the range 1668–1397 cm^{-1}, while in the type II structure these absorptions are in the range 1605–1381 cm^{-1} with two weak shoulders in the range 1665–1630 cm^{-1}. The IR spectrum of the La–SIP compound (type III) is nearly identical to that of the type II structure. However, the characteristic bands of the sulfonate group do not show any obvious change from type I to type III.

To assess the thermal stability of these compounds and their structural variation as a function of the temperature,

thermogravimetric analyses (TGA) were performed on single-phase polycrystalline samples of these materials (Figure S1). Since compounds of the same structure type show similar thermal behavior, the results of only three representative compounds − Yb (**2**) of type I, Tb (**7**) of type II, and La (**11**) of type III − are discussed. The TGA measurements for Yb (**2**) exhibit three distinct weight-loss steps. The first weight loss occurs between 60 and 110 °C due to the release of three lattice water molecules (weight loss: measured 9.55%; calculated 9.64%). The second weight loss in the temperature range 110–240 °C corresponds to the removal of the coordinated water molecules (observed 14.65%; calculated 16.07%). A further increase of the temperature leads to the decomposition of the compound at 540 °C. The thermogravimetric analysis of Tb (**7**) shows that the initial weight loss occurs in the temperature range 120–200 °C, attributable to the release of all coordinated water molecules (observed 14.67%; calculated 15.19%). The thermogravimetric analysis of La (**11**) indicates that the loss of the water (14.95%) takes place between 100 °C and 160 °C, corresponding to the release of all water molecules (calculated: 15.85%).

Conclusions

In conclusion, the self-assembly of the lanthanide series with a single (SIP) ligand with soft sulfonate probes leads to the formation of the unprecedented three structural types I (1D), II (2D), and III (3D). The compounds of the heaviest lanthanides (Lu, Yb, Tm, and Er) adopt a type I structure without Ln–sulfonate bonds, the Ho, Dy, Tb, Sm, Pr, and Nd compounds belong to type II, with one Ln–sulfonate bond, and the largest, La, forms a type III structure with two La–sulfonate bonds. The progressive structural changes resulting from the distinct preference for the lanthanide series to bind to anionic sulfonate groups are believed to due to their different basicity as a consequence of the effects of the lanthanide contraction. In addition, the SIP ligand displays diverse coordination modes, which together with the versatile coordination ability of the bridging ligand makes it adaptable to lanthanide ions of different sizes and leads to the various topologies of the coordination networks.

Experimental Section

General Remarks: All chemicals were purchased commercially and used without further purication, including 5-sulfoisophthalic acid monosodium salt (Alfa). Elemental analyses were carried out with an Elementar Vario EL III analyzer and IR spectra (KBr pellets) were recorded with a Perkin–Elmer Spectrum One. The thermogravimetric measurements were performed with a Netzsch STA449C apparatus under nitrogen with a heating rate of 10 °C min^{-1} from 25 to 800 °C. All complexes were synthesized by a hydrothermal method under autogenous pressure.

$[\{Lu(SIP)(H_2O)_5\}(H_2O)_3]_n$ (1): In a typical synthesis, solid Lu_2O_3 (0.04 g, 0.1 mmol) was dispersed in an aqueous solution (15 mL) of 5-sulfoisophthalic acid monosodium salt (0.03 g, 0.12 mmol) with a pH value of ca. 3–4. The mixture was placed in a Teflon-lined stainless-steel autoclave (30 mL), and the autoclave was sealed, heated to 160 °C under autogenous pressure for 5 d, and then cooled to room temperature at a rate of 6 °C h^{-1}. The resulting colorless, crystalline product was filtered, washed with distilled water, and dried at ambient temperature (0.035 g, yield 62% based on Lu). $C_8H_{19}LuO_{15}S$ (562.26): calcd. C 17.08, H 3.38; found C 17.01, H 3.33. IR (KBr pellet): $\tilde{\nu}$ = 3388(vs), 1664(s), 1612(vs), 1542(vs), 1460(s), 1396(vs), 1211(s), 1175(s), 1119(m), 1043(vs), 746(m), 628(s) cm^{-1}.

$[\{Yb(SIP)(H_2O)_5\}(H_2O)_3]_n$ (2): The synthetic procedure for **2** was similar to that for **1** but replacing Lu_2O_3 with Yb_2O_3. A colorless, crystalline product was obtained (0.042 g, yield 75% based on Yb). $C_8H_{19}O_{15}SYb$ (560.33): calcd. C 17.14, H 3.39; found C 17.00, H 3.36. IR (KBr pellet): $\tilde{\nu}$ = 3391(vs), 1667(s), 1614(vs), 1538(vs), 1462(s), 1397(vs), 1208(s), 1175(s), 1120(m), 1042(vs), 746(m), 628(s) cm^{-1}.

$[\{Tm(SIP)(H_2O)_5\}(H_2O)_3]_n$ (3): The synthetic procedure for **3** was similar to that for **1** but replacing Lu_2O_3 with Tm_2O_3. A pale-orange, crystalline product was obtained (0.037 g, yield 66% based on Tm). $C_8H_{19}O_{15}STm$ (556.22): calcd. C17.27, H 3.42; found C 17.19, H 3.41. IR (KBr pellet): $\tilde{\nu}$ = 3389(vs), 1667(s), 1614(vs), 1540(vs), 1460(s), 1395(vs), 1210(s), 1176(s), 1119(m), 1042(vs), 745(m), 628(s) cm^{-1}.

$[\{Er(SIP)(H_2O)_5\}(H_2O)_3]_n$ (4): The synthetic procedure for **4** was similar to that for **1** but replacing Lu_2O_3 with Er_2O_3. A pale-red, crystalline product was obtained (0.043 g, yield 78% based on Er). $C_8H_{19}ErO_{15}S$ (554.55): calcd. C17.31, H 3.43; found C 17.30, H 3.41. IR (KBr pellet): $\tilde{\nu}$ = 3391(vs), 1668(s), 1614(vs), 1538(vs), 1460(s), 1396(vs), 1210(s), 1176(s), 1120(m), 1042(vs), 745(m), 630(s) cm^{-1}.

$[\{Ho(SIP)(H_2O)_4\}]_n$ (5): The synthetic procedure for **5** was similar to that for **1** but replacing Lu_2O_3 with Ho_2O_3. A colorless, crystalline product was obtained (0.028 g, yield 59% based on Ho). $C_8H_{11}HoO_{11}S$ (480.16): calcd. C 20.04, H 2.29; found C 19.86, H 2.21. IR (KBr pellet): $\tilde{\nu}$ = 3390(vs), 3232(vs), 1658(w), 1642(w), 1605(vs), 1559(vs), 1458 vs), 1391(vs), 1208(m), 1180(s), 1115(w), 1042(s), 744(w), 628(m) cm^{-1}.

$[\{Dy(SIP)(H_2O)_4\}]_n$ (6): The synthetic procedure for **6** was similar to that for **1** but replacing Lu_2O_3 with Dy_2O_3. A colorless, crystalline product was obtained (0.030 g, yield 63% based on Dy). $C_8H_{11}DyO_{11}S$ (477.73): calcd. C 20.15, H 2.31; found C 20.14, H 2.25. IR (KBr pellet): $\tilde{\nu}$ = 3405(vs), 3232(vs), 1658(w), 1641(w), 1601(vs), 1538(vs), 1451(vs), 1382(s), 1223(m), 1206(m), 1180(s), 1116(w), 1043(s), 738(w), 620(m) cm^{-1}.

$[\{Tb(SIP)(H_2O)_4\}]_n$ (7): The synthetic procedure for **7** was similar to that for **1** but replacing Lu_2O_3 with Tb_4O_7. A colorless, crystalline product was obtained (0.031 g, yield 66% based on Tb). $C_8H_{11}O_{11}STb$ (474.15): calcd. C 20.25, H 2.32; found C 20.22, H 2.28. IR (KBr pellet): $\tilde{\nu}$ = 3391(vs), 3210(vs), 1664(w), 1639(w), 1602(vs), 1536(vs), 1458(vs), 1392(vs), 1208(m), 1177(m), 1116(m), 1042(s), 777(m), 742(m), 625(m) cm^{-1}.

$[\{Sm(SIP)(H_2O)_4\}]_n$ (8): The synthetic procedure for **8** was similar to that for **1** but replacing Lu_2O_3 with Sm_2O_3. A colorless, crystalline product was obtained (0.028 g, yield 61% based on Sm). $C_8H_{11}O_{11}SSm$ (465.58): calcd. C 20.65, H 2.36; found C 20.60, H 2.32. IR (KBr pellet): $\tilde{\nu}$ = 3408(vs), 3201(vs), 1653(w), 1634(w),

1602(vs), 1537(vs), 1448(vs), 1383(vs), 1222(vs), 1203(m), 1166(m), 1109(m), 1046(s), 773(m), 738(m), 630(m), 583(m) cm^{-1}.

$[\{Pr(SIP)(H_2O)_4\}]_n$ (9): The synthetic procedure for **9** was similar to that for **1** but replacing Lu_2O_3 with Pr_6O_{11}. A colorless, crystalline product was obtained (0.015 g, yield 34% based on Pr). $C_8H_{11}O_{11}PrS$ (456.14): calcd. C 21.05, H 2.41; found C 20.94, H 2.33. IR (KBr pellet): $\tilde{\nu}$ = 3410(vs), 3249(vs), 1650(w), 1633(w), 1601(vs), 1531(vs), 1447(vs), 1381(vs), 1223(vs), 1203(m), 1164(m), 1109(m), 1045(s), 773(m), 736(m), 627(m), 585(m) cm^{-1}.

$[\{Nd(SIP)(H_2O)_4\}]_n$ (10): The synthetic procedure for **10** was similar to that for **1** but replacing Lu_2O_3 with Nd_2O_3. A pink, crystalline product was obtained (0.024 g, yield 51% based on Nd).

Table 4. Crystallographic data for **1**–**5**.

	Lu (**1**)	Yb (**2**)	Tm (**3**)	Er (**4**)	Ho (**5**)
Empirical formula	$C_8H_{19}LuO_{15}S$	$C_8H_{19}O_{15}SYb$	$C_8H_{19}O_{15}STm$	$C_8H_{19}ErO_{15}S$	$C_8H_{11}HoO_{11}S$
Formula mass	562.26	560.33	556.22	554.55	480.16
Temperature [K]	273(2)	293(2)	293(2)	293(2)	293(2)
Crystal size [mm]	0.20×0.18×0.04	0.45×0.20×0.05	0.33×0.24×0.06	0.45×0.35×0.04	0.25×0.23×0.22
Space group	$P2_1/n$	$P2_1/n$	$P2_1/n$	$P2_1/n$	$Pna2_1$
Z	4	4	4	4	4
a [Å]	9.44700(10)	9.4630(5)	9.4681(17)	9.422(4)	7.2351(10)
b [Å]	10.4895(4)	10.5142(5)	10.5316(18)	10.526(4)	16.456(2)
c [Å]	17.1948(4)	17.2285(10)	17.252(3)	17.102(7)	10.3183(14)
β [°]	101.8210(10)	101.779(2)	101.8150(10)	101.312(4)	90
V [Å^3]	1667.77(8)	1678.07(15)	1683.8(5)	1663.2(11)	1228.5(3)
$D_{calcd.}$ [g cm^{-3}]	2.239	2.218	2.194	2.215	2.596
μ [mm^{-1}]	6.122	5.774	5.469	5.248	6.671
Measured reflections	5171	10289	12721	12505	8952
Independent reflections	2899	2953	3842	3816	2704
Observed reflections [$I > 2\sigma(I)$]	2276	2553	3593	3243	2603
Parameters	250	265	271	274	211
Completeness [%]	97.8	99.7	99.6	99.8	99.6
θ range [°]	2.94–25.08	2.99–25.03	2.28–27.48	2.28–27.48	2.33–27.48
hkl ranges	–10/11	–11/11	–12/11	–12/12	–9/8
	–6/12	–8/12	–13/13	–13/9	–21/16
	–20/20	–20/20	–22/12	–22/22	–12/13
R_1 (obsd. refl.)	0.0730	0.0348	0.0253	0.0306	0.0145
wR_2 (all refl.)	0.1739	0.0828	0.0611	0.0764	0.0337
Largest diff. peak/hole [e Å^{-3}]	1.761/–1.893	1.362/–2.349	1.551/–1.487	2.306/–1.162	0.615/–0.800

Table 5. Crystallographic data for **6**–**9** and **11**.

	Dy (**6**)	Tb (**7**)	Sm (**8**)	Pr (**9**)	La (**11**)
Empirical formula	$C_8H_{11}ODy_{11}S$	$C_8H_{11}O_{11}STb$	$C_8H_{11}O_{11}SSm$	$C_8H_{11}O_{11}PrS$	$C_8H_{11}LaO_{11}S$
Formula mass	477.73	474.15	465.58	456.14	454.14
Temperature [K]	273(2)	293(2)	273(2)	293(2)	273(2)
Crystal size [mm]	0.32×0.14×0.14	0.18×0.16×0.12	0.10×0.10×0.08	0.18×0.15×0.10	0.52×0.50×0.10
Space group	$Pna2_1$	$Pna2_1$	$Pna2_1$	$Pna2_1$	$P2_1/n$
Z	4	4	4	4	4
a [Å]	7.3006(7)	7.260(2)	7.2839(6)	7.1969(17)	7.9076(2)
b [Å]	16.6036(15)	16.508(5)	16.5781(14)	16.695(4)	15.2955(4)
c [Å]	10.4270(10)	10.353(3)	10.3919(8)	10.489(3)	10.4404(3)
β [°]	90	90	90	90	92.686(2)
V [Å^3]	1263.9(2)	1240.7(7)	1254.86(18)	1260.3(5)	1261.39(6)
$D_{calcd.}$ [g cm^{-3}]	2.511	2.538	2.464	2.404	2.391
μ [mm^{-1}]	6.136	5.928	4.905	4.091	3.611
Measured reflections	5968	9150	3814	9206	3907
Independent reflections	2190	2847	1602	2627	2274
Observed reflections [$I > 2\sigma(I)$]	1834	2634	1301	2490	2140
Parameters	147	214	142	214	208
Completeness[%]	99.7	99.8	99.9	99.8	98.4
2θ range[°]	2.31–25.06	2.47–27.48	2.31–25.09	3.08–27.48	2.36–25.35
hkl ranges	–8/7	–9/9	–8/8	–9/9	–9/8
	–17/9	–16/21	–19/14	–21/21	–15/18
	–12/12	–13/13	–6/12	–13/10	–8/12
R_1 (obsd. refl.)	0.0507	0.0267	0.0602	0.0225	0.0403
wR_2 (all refl.)	0.1276	0.0586	0.1354	0.0560	0.1013
Largest diff. peak/hole [e Å^{-3}]	1.945/–0.840	1.120/–0.701	1.113/–1.179	0.758/–0.556	1.298/–2.841

$C_8H_{11}NdO_{11}S$ (459.47): calcd. C 20.92, H 2.40; found C 20.88, H 2.36. IR (KBr pellet): $\tilde{\nu}$ = 3410(vs), 3251(vs), 1650(w), 1636(w), 1601(vs), 1534(vs), 1448(vs), 1382(vs), 1223(vs), 1204(m), 1167(m), 1109(m), 1049(s), 773(m), 737(m), 626(m), 583(m) cm^{-1}.

$[\{La(SIP)(H_2O)_3\}(H_2O)]_n$ (11): The synthetic procedure for **11** was similar to that for **1** but replacing Lu_2O_3 with La_2O_3. A colorless, crystalline product was obtained (0.035 g, yield 76% based on La). $C_8H_{11}LaO_{11}S$ (454.14): calcd. C 20.25, H 2.32; found C 20.24, H 2.30. IR (KBr pellet): $\tilde{\nu}$ = 3446(vs), 3218(vs), 1644(m), 1599(s), 1564(s), 1538(vs), 1451(s), 1436(s), 1378(vs), 1217(s), 1179(m), 1112(m), 1051(s), 775(m), 726(m), 619(m) cm^{-1}.

X-ray Crystallographic Study: X-ray diffraction data for complexes **2–5**, **7**, **9**, and **10** were collected with a Rigaku Mercury CCD diffractometer equipped with graphite-monochromated Mo-K_α radiation (λ = 0.71073 Å). The CrystalClear software package was used for data reduction and empirical absorption correction.[38] Data collection for complexes **1**, **6**, **8**, and **11** was performed with a Siemens Smart CCD diffractometer with graphite-monochromated Mo-K_α radiation (λ = 0.71073 Å). Empirical absorption corrections were applied using the SADABS program.[39] All structures were solved by direct methods and successive Fourier difference syntheses, and refined by the full-matrix least-squares method on F^2 (SHELXTL Version 5.1[40]). All non-hydrogen atoms were refined with anisotropic thermal parameters for all structures except **1**, **6**, and **8**. In the structures of **1**, **6**, and **8** all non-hydrogen atoms were refined anisotropically except several carbon and oxygen atoms, which were refined isotropically in order to prevent some of them being "non-positive-definite". Aromatic hydrogen atoms were assigned to calculated positions with isotropic thermal parameters fixed at 1.2-times that of the attached carbon atom. Some water hydrogen atoms were placed in calculated positions with isotropic thermal parameters fixed at 1.5-times that of the attached oxygen atom. Other water hydrogen atoms were located from difference maps and refined with O–H distances restrained to 0.95 Å, and isotropic thermal parameters fixed at 1.5-times that of the respective oxygen atom. The R_1 values are defined as $R_1 = \Sigma||F_o| - |F_c||/\Sigma|F_o|$ and $wR_2 = \{\Sigma[w(F_o^2 - F_c^2)^2]/\Sigma[w(F_o^2)^2]\}^{1/2}$. The crystallographic data for **1–11** (except **10**) are listed in Tables 4 and 5. Selected bond lengths together with some nonbonding interactions for **1–4**, **5–9**, and **11** are listed in Tables 1, 2, and 3, respectively. CCDC-267294 to -267303 (for **1–9** and **11**) contain the supplementary crystallographic data for this paper. These data can be obtained free of charge from The Cambridge Crystallographic Data Centre via www.ccdc.cam.ac.uk/data_request/cif.

Acknowledgments

We gratefully acknowledgment the financial support of the "One Hundred Talents Program" of the Chinese Academy of Sciences and National Science Foundation of China (grant no. 20473092).

[1] B. Moulton, M. J. Zaworotko, *Chem. Rev.* **2001**, *101*, 1629–1658.
[2] O. R. Evans, R. Xiong, Z. Wang, G. K. Wong, W. Lin, *Angew. Chem.* **1999**, *111*, 557–559; *Angew. Chem. Int. Ed.* **1999**, *38*, 536–538.
[3] D. L. Reger, T. D. Wright, R. F. Semeniuc, T. C. Grattan, M. D. Smith, *Inorg. Chem.* **2001**, *40*, 6212–6219.
[4] T. Bein, *Supramolecular Architecture*, American Chemical Society, Washington, DC, **1992**.
[5] O. Sato, T. Iyoda, A. Fujishima, K. Hashimoto, *Science* **1996**, *271*, 49–51.
[6] M. Fujita, Y. J. Kwon, S. Washizu, K. Ogura, *J. Am. Chem. Soc.* **1994**, *116*, 1151–1152.
[7] M. Munakata, L. P. Wu, T. Kuroda-Sowa, M. Maekawa, Y. Suenaga, K. Furuichi, *J. Am. Chem. Soc.* **1996**, *118*, 3305–3306.
[8] Y. C. Liang, M. C. Hong, R. Cao, J. B. Weng, W. P. Su, *Inorg. Chem.* **2001**, *40*, 4574–4582.
[9] J. H. Yang, S. L. Zheng, X. L. Yu, X. M. Chen, *Cryst. Growth Des.* **2004**, *4*, 831–834.
[10] X. M. Zhang, H. S. Wu, X. M. Chen, *Eur. J. Inorg. Chem.* **2003**, 2959–2964.
[11] S. H. Feng, R. R. Xu, *Acc. Chem. Res.* **2001**, *34*, 239–247.
[12] C. Ruiz-Pérez, P. A. Lorenzo-Luis, M. Hernández-Molina, M. M. Laz, F. S. Delgado, P. Gili, M. Julve, *Eur. J. Inorg. Chem.* **2004**, 3873–3879.
[13] S. K. Ghosh, G. Savitha, P. K. Bharadwaj, *Inorg. Chem.* **2004**, *43*, 5495–5497.
[14] S. K. Ghosh, R. Joan, P. K. Bharadwaj, *Cryst. Growth Des.* **2005**, *5*, 623–629.
[15] D. F. Sun, R. Cao, Y. Q. Sun, W. H. Bi, D. Q. Yuan, Q. Shi, X. Li, *Chem. Commun.* **2003**, 1528–1529.
[16] D. F. Sun, R. Cao, Y. Q. Sun, X. Li, W. H. Bi, M. C. Hong, Y. J. Zhao, *Eur. J. Inorg. Chem.* **2003**, 94–98.
[17] J. Tao, X. Yin, Z. B. Wei, R. B. Huang, L. S. Zheng, *Eur. J. Inorg. Chem.* **2004**, 125–133.
[18] Z. M. Sun, J. G. Mao, Y. Q. Sun, H. Y. Zeng, A. Clearfield, *Inorg. Chem.* **2004**, *43*, 336–341.
[19] D. S. Kim, P. M. Forster, R. L. Toquin, A. K. Cheetham, *Chem. Commun.* **2004**, 2148–2149.
[20] S. K. Ghosh, P. K. Bharadwaj, *Inorg. Chem.* **2004**, *43*, 2293–2298.
[21] D. M. L. Goodgame, S. P. W. Hill, D. J. Williams, *Inorg. Chim. Acta* **1998**, *272*, 131–140.
[22] C. V. K. Sharma, R. D. Rogers, *Chem. Commun.* **1999**, 83–84.
[23] X. J. Zheng, Z. M. Wang, S. Gao, F. H. Liao, C. H. Yan, L. P. Jin, *Eur. J. Inorg. Chem.* **2004**, 2938–2973.
[24] L. Tei, A. J. Blake, C. Wilson, M. Schröder, *Dalton Trans.* **2004**, 1945–1952.
[25] P. C. R. Soares-Santos, T. Trindade, A. C. Tomé, J. Rocha, R. A. Sá Ferreira, L. D. Carlos, F. A. A. Paz, J. Klinowski, H. I. S. Nogueira, *New J. Chem.* **2004**, *28*, 1352–1358.
[26] L. Pan, X. Y. Huang, J. Li, Y. G. Wu, N. W. Zheng, *Angew. Chem. Int. Ed.* **2000**, *39*, 527–530.
[27] X. Li, Q. Shi, D. F. Sun, W. H. Bi, R. Cao, *Eur. J. Inorg. Chem.* **2004**, *4*, 2747–2753.
[28] Z. He, E. Q. Gao, Z. M. Wang, C. H. Yan, M. Kurmoo, *Inorg. Chem.* **2005**, *44*, 862–874.
[29] Z. Wang, M. Strobele, K. L. Zhang, H. J. Meyer, X. Z. You, Z. Yu, *Inorg. Chem. Commun.* **2002**, *5*, 230–234.
[30] R. M. Barrer, *Hydrothermal Chemistry of Zeolite*, Academic Press, London, **1982**.
[31] G. Bemazeau, *J. Mater. Chem.* **1999**, *9*, 15–18.
[32] S. H. Feng, R. R. Xu, *Acc. Chem. Res.* **2001**, *34*, 239–247.
[33] Q. Y. Liu, L. Xu, *Inorg. Chem. Commun.* **2005**, *8*, 401–405.
[34] Q. Y. Liu, L. Xu, *CrystEngComm* **2005**, *7*, 87–89.
[35] A. Onoda, Y. Yamada, M. Doi, T. Okamura, N. Ueyama, *Inorg. Chem.* **2001**, *40*, 516–521.
[36] T. Moeller, *The Chemistry of the Lanthanides*, Pergamon Press, New York, **1975**.
[37] G. Socrates, *Infrared Characteristic Group Frequencies*, John Wiley & Sons, Stonebridge Press, Bristol, **1980**.
[38] *CrystalClear version 1.3*, Rigaku Corp., **2000**.
[39] G. M. Sheldrick, *A program for the Siemens Area Detector ABSorption correction*, University of Göttingen, **1997**.
[40] G. M. Sheldrick, *SHELXS 97*, *Program for Crystal Structure Solution*, University of Göttingen, **1997**.

Received: March 30, 2005
Published Online: August 1, 2005

